Journal of Materials Chemistry A

PAPER

View Article Online
View Journal

Cite this: DOI: 10.1039/c6ta01353h

Transparent conducting oxide-free and Pt-free flexible dye-sensitized solar cells employing CuS-nanosheet networks as counter electrodes†

Xiaojia Zhang,[a] Wenxi Guo*[ab] and Caofeng Pan*[a]

Received 14th February 2016
Accepted 29th March 2016

DOI: 10.1039/c6ta01353h

www.rsc.org/MaterialsA

We present completely transparent conducting oxide (TCO)-free and platinum (Pt)-free flexible dye sensitized solar cells (DSSCs) with remarkable efficiency and superior mechanical flexibility, consisting of TiO_2 nanotube arrays on Ti foil (TNARs/Ti) as the photoanode and newly designed free-standing copper sulphide nanosheet (CuS NS) networks as the counter electrode (CE). Herein, CuS NS networks not only served as conducting films, but also as catalysts for DSSCs. CuS NS network electrodes exhibit both excellent optoelectronic performances (a sheet resistance of 20 Ω sq^{-1} at 80% transmittance) and remarkable mechanical stability under bending tests compared to traditional ITO/plastic substrates. What is more, the electrochemical catalytic activity of CuS NS networks towards triiodide solution was first investigated and 6.38% energy conversion efficiency was obtained by using CuS NS networks as the CE.

Introduction

With the rapid development of smart, portable and light-weight electronic products, flexible and even foldable energy harvesting and energy storage devices have become an increasing research hotspot for scientific research and manufacturing technology.[1–3] As an environmentally friendly energy resource, dye-sensitized solar cells (DSSCs) have received a great deal of attention and worldwide interest due to their high absorption efficiency and low-cost fabrication.[4,5] In recent years, tremendous efforts have been made to promote traditional rigid DSSCs into flexible ones, which would enable roll-to-roll processes and reduce the production costs in high-volume manufacturing.[6–11] In the fabrication of DSSCs, high-quality crystalline photoanodes are usually obtained by high-temperature calcination, thus a major challenge preventing DSSCs towards flexible application is the temperature limitation of the plastic substrates.[11–16] To address this problem, a back-side illumination configuration typically including the photoanode on a heat-resistant metal foil or fibers (opaque) and the counter electrode (CE) on a transparent polymer substrate has been designed.[8,10,17–20] Although tremendous efforts have been made to improve the flexibility of this kind of DSSC, three key issues still need to be resolved. First of all, the mechanical flexibility of the electrodes needs to be further improved. The widely used indium tin oxide (ITO) film in flexible DSSCs is brittle and its conductivity is sensitive to mechanical deformation, preventing it from extensive applications in flexible electronics.[21] Secondly, highly conducting transparent CEs with high electrochemical catalytic activity are not easily achieved.[22–28] Although Pt and most of the carbon-based CEs exhibit excellent catalytic activity towards the reduction of triiodide, their optical transparency is not ideal according to the benchmark parameters for ideal CE function (carbon black ~ 14.47 μm, carbon nanotubes ~ 5 μm, graphite ~ 9 μm).[29–32] Thirdly, the cost of the Pt and transparent conductive oxide (TCO) glass commonly used in DSSCs is more than 40% of the total device cost,[29,33] which makes them not suitable for large scale applications. To satisfy all the aforementioned requirements, tremendous efforts have been made to design and fabricate TCO-free and Pt-free electrodes for DSSCs, such as conductive polymers, metal grids, conductive fibers and carbon materials.[34–42]

Here we present novel, completely TCO-free and Pt-free DSSCs comprising TiO_2 nanotube arrays on Ti foil (TNARs/Ti) as the photoanode and the newly designed CuS NS networks as the CE, which exhibit remarkable efficiency and long-term stability. CuS NS networks not only served as conducing films, but also as catalysts for DSSCs. CuS NS network electrodes exhibit both excellent optoelectronic performances (a sheet resistance of 20 Ω sq^{-1} at 80% transmission) and remarkable mechanical stability under bending tests compared to the commercial ITO/plastic substrates. Moreover, the electrochemical catalytic activity of CuS NS networks towards the triiodide electrolyte was first investigated and 6.38% energy conversion efficiency was obtained by using CuS NS networks as the CE. Due to the elimination of ITO and Pt, the production cost of this kind of DSSC can be further reduced. The superior durability of the CuS

[a]Beijing Institute of Nanoenergy and Nanosystems, Chinese Academy of Sciences, Beijing, China. E-mail: cfpan@binn.cas.cn

[b]Research Institution for Biomimetics and Soft Matter and Department of Physics, Xiamen University, Xiamen, 361005, PR China. E-mail: wxguo@xmu.edu.cn

† Electronic supplementary information (ESI) available: Supplementary XRD, TEM, SEM or other electronic formats. See DOI: 10.1039/c6ta01353h

NS network electrodes could greatly enhance the flexibility of the DSSCs. We believe that the CuS NS network electrode with excellent conductivity, transparency, mechanical stability, and superior chemical catalytic capability will broaden the applications of the flexible DSSCs and also can be used in the areas of optoelectronic devices, flexible electronics and sensors.

Experimental

Materials

Polyvinyl alcohol (PVA), sulphur, ethanol, titanium tetrachloride, acetonitrile, $H_2PtCl_6 \cdot 6H_2O$, 2-propanol, NH_4F and methanol were purchased from Sinopharm Chemical Reagent Co. Ltd and all these reagents are analytically pure. LiI, I_2, 4-tertbutylpyridine, and Ti foil were purchased from Sigma Aldrich. N719 dye was purchased from Solaronix.

CuS NS network fabrication

First of all, transparent Cu networks were fabricated on different flexible substrates by means of electrospinning templates and magnetron sputtering as reported by Cui *et al.*:[43] free-standing PVA fibers were spun on an aluminum frame to form a network and then a thin layer of Cu film with a thickness of 50–100 nm was deposited on the free-standing PVA fibers by magnetron sputtering. The Cu networks were derived after transferring the whole structure onto the polyethylene terephthalate (PET) substrate and removing the PVA nanofibers by submerging the whole electrode into water or ethanol for a few seconds. Second, the Cu network electrode was submerged into saturated sulfur–ethanol solution at 60 °C for 6–24 h, until all the Cu networks were transferred into CuS and the CuS nanotrough network electrode was obtained.

The fabrication of the platinized FTO electrode

Typically, a platinized FTO CE was prepared by spreading a drop of 7 mM of $H_2PtCl_6 \cdot 6H_2O$ in 2-propanol on FTO glass, followed by drying at ambient temperature and annealing at 400 °C for 20 min.

TiO_2 nanotube array (TNAR) fabrication

TNARs on Ti foil were fabricated by a two-step electrochemical anodization process.[7] In brief, ethylene glycol solution containing 0.3 wt% NH_4F and 2 vol% H_2O was used as the electrolyte, and then the first-step anodization was performed at 50 V for 9–12 h with a cleansed Ti foil as the working electrode and a Pt foil as the CE. Subsequently, the as-prepared TANRs were peeled off by ultrasonic cleaning for a few minutes. Then, the obtained Ti foil was anodized again under the same circumstance for another 2–3 h to fabricate highly ordered TNARs. A high temperature annealing was performed at a temperature of 450 °C for 2 h in the air. Finally, the annealed TNARs/Ti foil was treated with 0.2 M $TiCl_4$ aqueous solution at 70 °C for 30 min, followed by heating at 450 °C for 2 h to enhance the surface area.

The preparation of DSSCs and photovoltaic characterization

The TNARs on Ti foil photoanodes were immersed in 0.5 mM N719 dye ethanol solution for 24 h and washed with ethanol to remove the unanchored dye. The aforementioned TNARs and CEs (platinized FTO, Cu and CuS NS network electrodes) were assembled together by using a hot-melt sealing tape as the spacer (SX1170-25; Solaronix Co.) The electrolytes including 0.5 M LiI, 50×10^{-3} M I_2, and 0.5 M 4-tertbutylpyridine in 3-methoxypropionitrile (Fluka) were employed for DSSCs. The photocurrent measurement was done under the AM 1.5 G (Newport) condition. The electrochemical impedance measurements were carried out with an Autolab (model ATU84315) and the IPCE was measured by using an IPCE measurement (Newport).

Characterization

All the films' sheet resistances were measured by using a digital multimeter (Keithley 2100) with a four-point probe. The optical transmittance of the network electrodes and ITO/PET films was measured by UV-vis spectroscopy (Shimadzu UV-3600). The morphology and structure of the flexible electrodes were characterized by field emission scanning electron microscopy (FESEM, HITACHI S8000) and high-resolution transmission electron microscopy (HRTEM, F20, 200 kV). The phase identification of the hybridized electrodes was conducted by X-ray diffraction (XRD) using a PANalytical X'Pert PRO diffractometer.

Results and discussion

Fig. 1a displays the scheme for the fabrication of the CuS NS network transparent conductive electrode. To fabricate CuS NS networks, Cu nanotrough networks were first constructed on the flexible substrates by electrospinning and magnetron sputtering as previously reported by Cui *et al.*[43] Then, the CuS NS networks were obtained by submersing the as-prepared Cu nanotrough networks in the ethanol solution, containing excessive sulfur powders, at 60 °C for several hours, until all the Cu was transformed into CuS. In Fig. 1b, the transmittance and conductivity of the network electrodes were related to the number of layers of transferred nanotroughs. The more layers transferred to the substrate, the less transparency and better conductivity achieved. Additional sheet resistance *versus* transmittance performances of Cu and CuS NS networks on PET substrates are plotted in Fig. 1b and S1,† respectively. It is apparent that the electrical conductivity of the CuS networks decreased compared to that of the Cu networks as expected, and ~90% light transmittance was achieved with the sheet resistance less than 5 $\Omega\ sq^{-1}$ and 40 $\Omega\ sq^{-1}$ for Cu and CuS networks, respectively. Despite this, to the best of our knowledge, our flexible CuS network films exhibit much better optoelectronic performances than previously reported CuS films which are generally fabricated on rigid substrates by means of magnetron sputtering.[44–46]

It is worth noting that the optical transmittance was only slightly decreased at the wavelengths from 400 nm to 800 nm after converting into CuS networks as shown in Fig. S2.† As

presented in Fig. 1c, the length of the CuS NSs can achieve several centimeters and interconnect with each other through a junction between two CuS NSs. Compared to metal nanowire network electrodes, long CuS NS networks can effectively minimize the number of wire-to-wire junctions, and exhibit small junction resistance. The photograph in Fig. 1d shows a 4 × 4 cm flexible transparent CuS NS network electrode, indicating that the reddish orange Cu networks were converted into neutral-gray CuS. Fig. 1d shows the SEM and optical images of the as-prepared CuS NS networks; it is obvious that all the NSs were uniformly covered by sheet-like nanoplates with a side length of ~1.5 μm and a thickness of ~50 nm. In Fig. 1e, the optoelectronic performances of CuS NS networks on PET can be compared to those of the traditional transparent conductive electrodes, *e.g.* FTO glass, ITO glass, platinized FTO with great transmittance and conductivity. What is more, the CuS NS networks can be fabricated on different flexible substrates at low temperatures without damaging the substrates. Fig. 1f shows some examples in which CuS NS networks were successfully fabricated onto various flexible substrates, including PET, paper, Kapton and tape, respectively.

To identify the characteristics of the as-prepared CuS NS network electrodes, X-ray diffraction (XRD) and transmission electron microscopy (TEM) were performed. Compared to XRD patterns of pure Cu networks in Fig. S3,† new diffraction peaks were located at 27.6°, 29.3°, 31.8°, 32.6°, 48.1°, 52.7° and 59.2° and appeared after 12 h reaction. According to JCPDS card no. 06-0464, these peaks can be readily indexed to (101), (102), (103), (006), (110), (108) and (116) of a pure hexagonal CuS phase. Furthermore, the crystal structure of a CuS NS was analyzed by TEM, high-resolution transmission electron microscopy (HRTEM) and the corresponding selected area electron diffraction (SAED) patterns as shown in Fig. S3.†

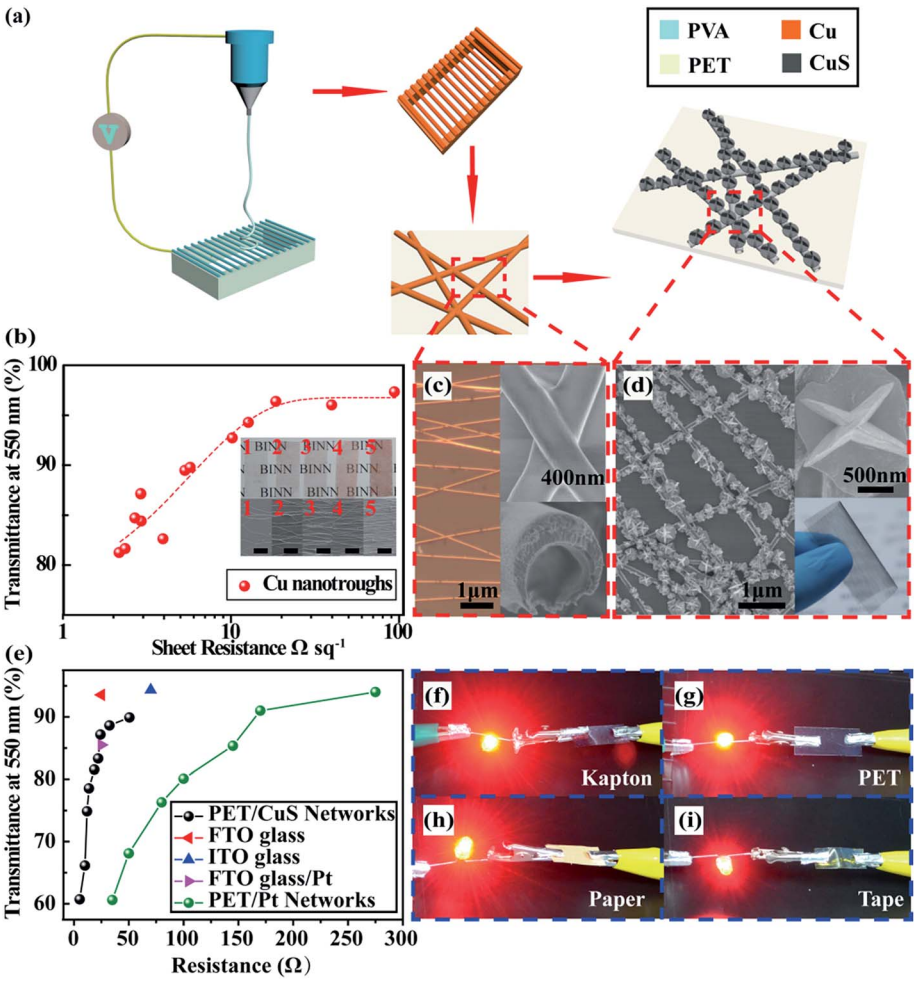

Fig. 1 Scheme for fabrication and characteristics of the CuS NS network transparent conductive electrode. (a) Fabrication processes of the CuS NS networks: electrospinning the polymer fibers on the as-prepared Al foil collector, and then a thin layer of copper is deposited on the PVA fibers by magnetron sputtering, finally the obtained Cu network electrodes are immersed in sulfur solution and transformed into CuS NS networks. (b) The transmittance *vs.* sheet resistance (at 550 nm) of the Cu networks with different layers; the insets are corresponding photographs and SEM images of the Cu network electrodes and the scale bar is 200 μm. (c) The optical microscopy photos and SEM images of the Cu network electrodes; (d) the photos and SEM images of the CuS NS network electrodes. (e) The transmittance *vs.* sheet resistance of the PET/CuS NS networks, FTO/glass, ITO/glass, FTO/glass/Pt (platinized FTO) and PET/Pt networks. (f)–(i) The photographs of the CuS NS networks are constructed on different substrates: Kapton (f); PET (g); paper (h); tape (i).

The lattice spacing of 0.314 nm matches well with the interplanar spacing (101) planes of the hexagonal CuS phase and the corresponding SAED pattern obtained from the red area in Fig. S3† shows several diffraction points, which can be indexed to the (101) and (011) lattice planes of the hexagonal phase of CuS as well. According to the aforementioned data, the as-prepared CuS NSs were well crystallized.

To investigate the performance of the CuS NS network electrodes in the application of DSSCs as CEs, we studied the electrocatalytic abilities of the CuS NS network electrode by cyclic voltammetry (CV) measurements. All the CV curves were obtained in the electrolyte, containing 10.0 mM LiI, 1.0 mM I_2, and 0.1 mM $LiClO_4$ in acetonitrile (ACN) at a scan rate of 50 mV s^{-1}, where the corresponding redox reaction can be expressed by the equation ($3I^- \leftrightarrow I_3^- + 2e^-$). Here, as a comparison, pure Cu networks on PET and semitransparent platinized FTO glass achieved by thermal decomposition at 400 °C were introduced. Fig. 2a compares the CV curves of the Cu networks, platinized FTO and CuS NS networks. It is obvious that no redox peaks appear on the CV curve for the Cu network electrode, indicating its poor electrocatalytic ability towards the I_3^- reduction. Conversely, obvious reductive peaks are observed at the interval of −0.3 to −0.4 V for both CuS NS networks and platinized FTO electrodes, indicating that the CuS network electrode exhibits excellent electrocatalytic activity in the application of DSSCs. The superior catalytic ability of the CuS NS networks may be ascribed to the following factors. First, the CuS NS network and sheet-like structures provide a relatively larger active surface area for I_3^- reduction. Second, the specific open channels of hollow-core CuS benefit the diffusion of I_3^-/I^- redox species.[47] Finally, due to the excellent electrical conductivity and superior catalytic performance, the CuS CEs can eliminate the catalyst/TCO film interface which may introduce the possibility of the electron–hole recombination.

In order to verify the chemical stability of CuS networks in DSSCs as the CE, long-term stability measurement was performed in the same I_3^-/I^- redox electrolyte at a scan rate of 50 mV s^{-1}. In Fig. 2b, the CV curve after 50 cycles of scan shows only a 5% decrease in the cathodic peak current density. The insets in Fig. 2b show that the morphology of the microflower composed of CuS NSs before and after polarization remains the same. There is a dramatic decrease in redox currents after 10 cycles as shown in Fig. S4,† revealing that the Cu networks exhibit poor chemical stability in the I_3^-/I^- electrolyte. Although Cu networks are one of the promising next generation transparent conducing electrodes (TCEs) to replace ITO, their easy oxidation would limit large scale applications in optoelectronic devices. The superb chemical stability and remarkable electrochemical catalytic ability of our CuS NS TCE just remedy those weaknesses and would greatly promote the development of the TCE network. To investigate the CEs' electrocatalytic kinetics, electrochemical impedance spectroscopy (EIS) is performed and the resultant Nyquist plots are illustrated in Fig. 2c. The Nyquist plots are fitted to the equivalent circuit model and the obtained EIS parameters are summarized in Table 1. The electrocatalytic resistance at the interface between

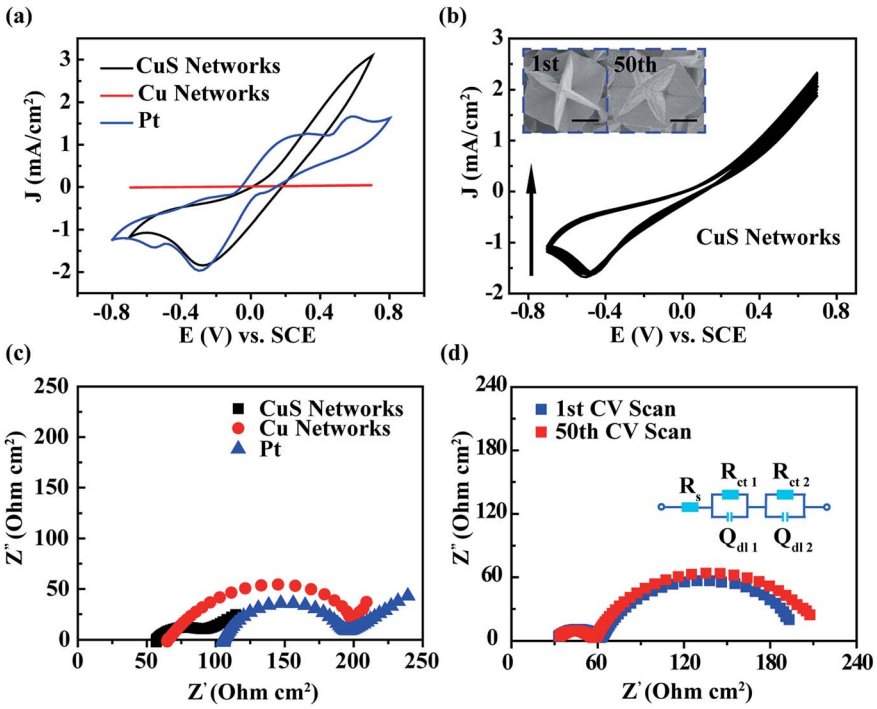

Fig. 2 (a) CV curves of the CEs with the film of the Cu, CuS NS network and platinized FTO electrodes obtained in acetonitrile solution containing 10.0 mM LiI, 1.0 mM I_2, and 0.1 M $LiClO_4$, at a scan rate of 50 mV s^{-1}, respectively; (b) CV curves of the CEs with the CuS NS network electrodes obtained for 50 cycles in the same electrolyte at a scan rate of 50 mV s^{-1}; (c) EIS curves of the Cu, CuS NS network and platinized FTO electrodes in the same electrolyte; (d) EIS curves of the CuS NS network electrodes before and after polarization in the same electrolyte.

the electrolyte and the CEs (R_{ct}) is associated with the electrocatalytic ability. Generally, the R_{ct} value at the CE/electrolyte interface is directly proportional to the over potential for the electron transfer from the CE to the I_3^- species.[48,49] From Table 1, the R_{ct} of the CuS NS electrode is 21.95 Ω cm^{-2}, and is smaller than that of the Cu network electrode (1259 Ω cm^{-2}) and the platinized FTO electrode (36.71 Ω cm^{-2}), indicating excellent electrochemical catalytic ability of the CuS NS network electrode. After 50 cycles of CV scan, the R_{ct} value of the Cu network electrode increased to 14 660 Ω cm^{-2}, a dramatic increase compared to the value before polarization, as shown in Fig. S5.† As for the CuS NS network electrode before and after 50 scan cycles, no obvious changes can be observed in the Nyquist plots as shown in Fig. 2d. The CuS NS network electrodes as the CEs in DSSCs are a promising alternative to Pt or other materials, *e.g.* graphene, carbon and conducting polymers.

Fig. 3a illustrates the schematic structure and the corresponding photograph of a flexible DSSC fabricated with TNARs as the photoanode and the CuS NS network as the CE. The SEM image in Fig. 3a shows the top and side-views of TNARs. Fig. 3b and c show the current density (J)–voltage (V) characteristics of DSSCs based on the platinized FTO, Cu and CuS NS networks as CEs, respectively. The photovoltaic parameters are listed in Table 1, illustrating that the J_{sc}, V_{oc} and FF of the DSSCs based on CuS NS networks are 18.10 mA cm^{-2}, 0.66 V and 0.53, respectively, yielding a power conversion efficiency (PCE) of 6.38%, which is even higher than that of DSSCs based on platinized FTO CEs (5.6%), while the Cu network electrode shows quite low photovoltaic efficiency as shown in Fig. 3c. The IPCE curves of the three kinds of electrodes are shown in Fig. 3d. In the wavelength range between 400 nm and 800 nm, the peak value for the CuS NS network electrode is as high as 89.9%, while those for the platinized FTO and Cu network electrodes are 70% and 20%, respectively. The results match well with the tendency of the efficiencies shown in Fig. 3b and c.

Table 1 Photovoltaic parameters of the DSSCs based on platinized FTO, Cu networks and CuS NS networks, and results of the EIS fitting using the electrical equivalent circuit model in Fig. 2d

Sample	J_{sc} [mA cm^{-2}]	V_{oc} [V]	PCE [%]	FF	R_{ct} [Ω cm^{-2}]
Platinized FTO	15.81	0.70	5.60	0.506	36.71
Cu network	0.0085	0.086	0.000183	0.342	1529
CuS NS network	18.10	0.66	6.38	0.534	21.95

In addition, CuS NS network electrodes show a wider diaphanous window than commercial ITO or FTO films. Fig. S6† displays the transmittance spectra of the Cu and the CuS NS network electrodes, commercial FTO/glass and ITO/glass electrodes from 400 nm to 2000 nm. Both the Cu and CuS NS network electrodes demonstrated high transparency to near-infrared light and presented a flat spectrum for the entire wavelength range from 400 to 2000 nm while the transmittances of commercial FTO/glass and ITO/glass electrodes demonstrated a sharp decrease in the transmittance spectra in the near-infrared wavelength from 1000 nm to 2000 nm. The superior transparency of the CuS NS network electrode could be used in near-infrared solar cells.

The mechanical durability of the electrodes and the thus assembled DSSCs were tested by periodic bending and releasing

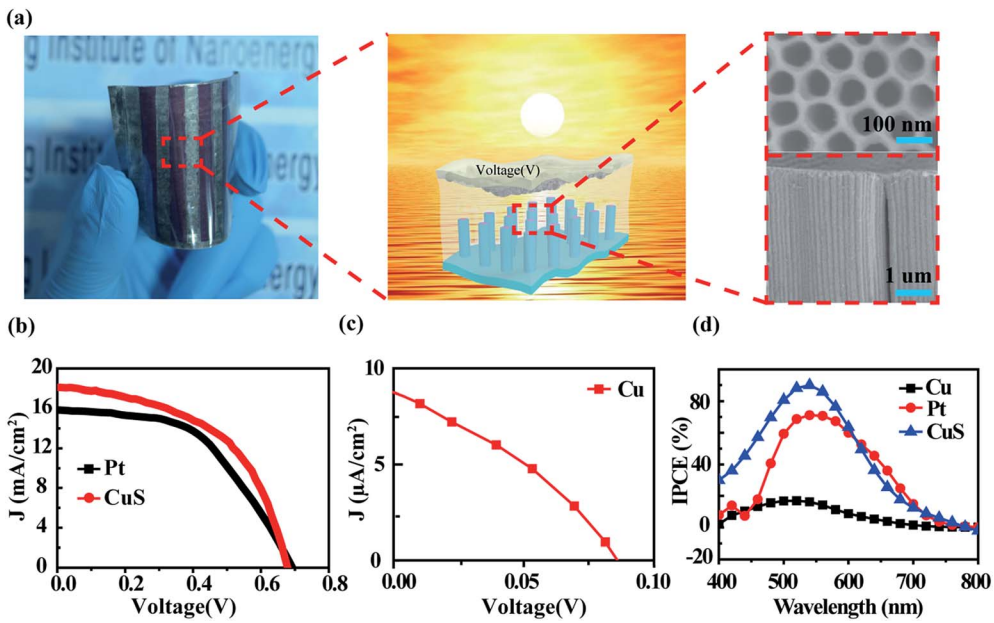

Fig. 3 (a) A photograph and the corresponding schematic illustration of the DSSC with the CuS NS network electrode as the CE and the TNARs/Ti foil the photoanode; SEM images of the morphology of the TNARs from the top and the cross section; (b) J–V curves of the DSSCs with films of the CuS NS networks and platinized FTO as CEs, respectively, under a light intensity of 100 mW cm^{-2}; (c) J–V curves of the DSSCs employing the Cu network electrodes under a light intensity of 100 mW cm^{-2}; (d) incident photo-to-current conversion efficiency (IPCE) curves of the flexible DSSCs employing the platinized FTO, Cu and CuS NS networks as CEs, respectively.

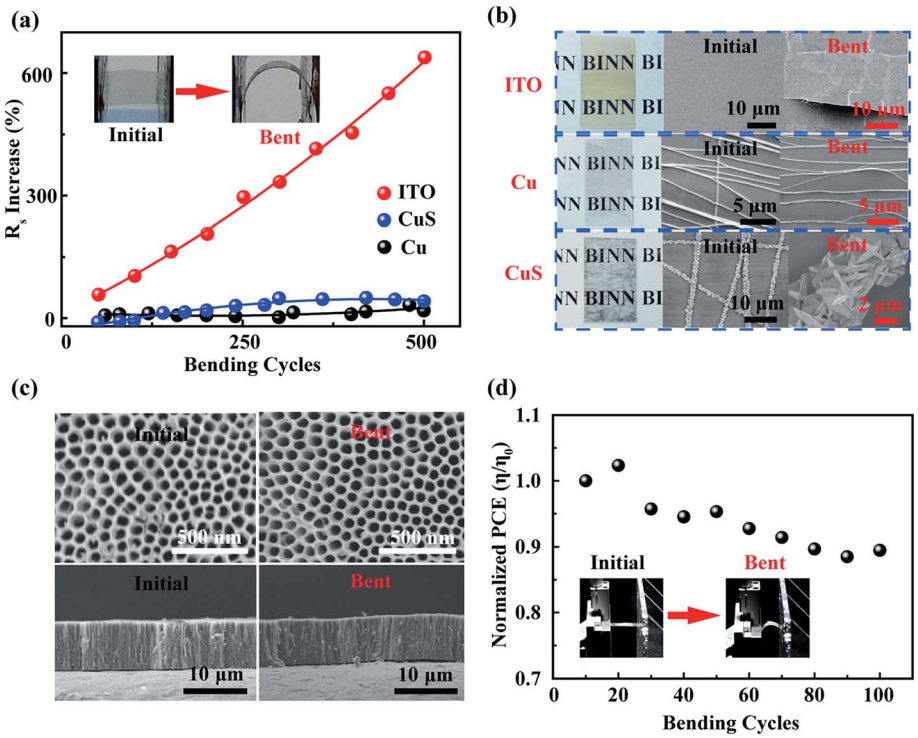

Fig. 4 (a) Resistance increase according to the number of cyclic bending of the Cu, CuS NS network electrodes and the commercial ITO electrode, respectively; the insets show the minimum and maximum bending deformation of the CuS NS network electrode. (b) SEM images before and after bending tests with the Cu, CuS NS network electrodes and the commercial ITO/PET electrodes at different scale bars; the photographs of these three electrodes after bending tests are also shown. (c) SEM images of the surface and the cross-sectional morphology of the TNARs before and after the bending tests; (d) Normalized PCE (η/η_0) of the CuS NS-based flexible DSSCs as a function of bending cycles with 50 mm bending radius; the insets are the photos of the initial and the bent configurations.

using a linear motor. First, the Cu and CuS NS network electrodes, and commercial ITO/PET electrodes were further investigated under cyclic bending deformation as shown in the inset in Fig. 4a. Obviously, both the Cu and CuS NS network electrodes exhibited remarkable mechanical stability and only negligible increase in sheet resistance after the bending test, while that of the ITO/PET electrode increased sharply and the sheet resistance was increased over 600% after bending tests. Fig. 4b shows the SEM images of the Cu networks, CuS networks and ITO/PET film before and after bending tests. It is obvious that no cracks were observed on the surface of the CuS NSs after 500 bending cycles, while the ITO film broke into pieces. This superior mechanical stability is attributed to the inherent resilience of the CuS NSs and their strong adhesion to the PET substrates. The impressive mechanical properties of CuS NSs could expand their applications in flexible solar cells and skin-like sensors. Secondly, the mechanical flexibility of the annealed TNARs was also investigated here by periodic bending and releasing. Fig. 4c presents the SEM images of TNARs on Ti foil before and after bending tests, no obvious cracks and falling off were observed. We found out that the annealing process would greatly enhance the adhesion and strength of the TNAR film. Finally, the mechanical flexibility of the DSSCs based on CuS networks and sensitized TNRAs was also investigated by the same method. Fig. 4d shows the relative conversion efficiency (η_1/η_0) at different bending cycles and a ~10% decrease after 100 cycles of bending and relaxing.

Conclusion

In summary, we have successfully fabricated TCO-free and Pt-free flexible DSSCs employing the CuS NS network electrodes as the CE. The CuS NS network electrode not only exhibits superior conductivity and transparency, but also achieves excellent mechanical ability and electrochemical catalytic ability compared to the commercial ITO/PET substrates. A PCE of 6.38% was achieved for the DSSC employing an optimized CuS NS network CE, suggesting a 14% increase in PCE as compared to the devices fabricated by the platinized FTO CE. Moreover, bending tests show a ~10% efficiency decrease after 100 cycles of bending and relaxing. The low-cost CuS NS networks with highly transparent conductivity, excellent mechanical and chemical stability and superior catalytic properties could promote the development of flexible electronic devices.

Acknowledgements

The authors are thankful for support from the "Thousand Talents" program of China for pioneering researchers and innovative teams and from the President Funding of the Chinese Academy of Sciences, National Natural Science Foundation of China (No. 51432005, 61405040, 61505010 and 51502018, 51502253), Beijing City Committee of science and

technology (Z151100003315010) and fundamental Research Funds for the Central Universities of China (20720150030).

References

1 M. Z. Liu, M. B. Johnston and H. J. Snaith, *Nature*, 2013, **501**, 395–398.
2 S. Xu, Y. H. Zhang, L. Jia, K. E. Mathewson, K. I. Jang, J. Kim, H. R. Fu, X. Huang, P. Chava, R. H. Wang, S. Bhole, L. Z. Wang, Y. J. Na, Y. Guan, M. Flavin, Z. S. Han, Y. G. Huang and J. A. Rogers, *Science*, 2014, **344**, 70–74.
3 X. D. Wang, H. L. Zhang, R. M. Yu, L. Dong, D. F. Peng, A. H. Zhang, Y. Zhang, H. Liu, C. F. Pan and Z. L. Wang, *Adv. Mater.*, 2015, **27**, 2324–2331.
4 M. Gratzel, *J. Photochem. Photobiol., C*, 2003, **4**, 145–153.
5 B. Oregan and M. Gratzel, *Nature*, 1991, **353**, 737–740.
6 K. Yoo, J. Y. Kim, J. A. Lee, J. S. Kim, D. K. Lee, K. Kim, J. Y. Kim, B. Kim, H. Kim, W. M. Kim, J. H. Kim and M. J. Ko, *ACS Nano*, 2015, **9**, 3760–3771.
7 W. X. Guo, C. Chen, M. D. Ye, M. Q. Lv and C. J. Lin, *Nanoscale*, 2014, **6**, 3656–3663.
8 H. C. Weerasinghe, F. Z. Huang and Y. B. Cheng, *Nano Energy*, 2013, **2**, 174–189.
9 W. X. Guo, F. Zhang, C. J. Lin and Z. L. Wang, *Adv. Mater.*, 2012, **24**, 4761–4764.
10 D. Garcia-Alonso, V. Zardetto, A. J. M. Mackus, F. De Rossi, M. A. Verheijen, T. M. Brown, W. M. M. Kessels and M. Creatore, *Adv. Energy Mater.*, 2014, 4.
11 W. Guo, X. Xue, S. Wang, C. Lin and Z. L. Wang, *Nano Lett.*, 2012, **12**, 2520–2523.
12 Y. J. Kim, M. H. Lee, H. J. Kim, G. Lim, Y. S. Choi, N. G. Park, K. Kim and W. I. Lee, *Adv. Mater.*, 2009, **21**, 3668–3673.
13 J. J. Lin, A. Nattestad, H. Yu, Y. Bai, L. Z. Wang, S. X. Dou and J. H. Kim, *J. Mater. Chem. A*, 2014, **2**, 8902–8909.
14 W. X. Guo, C. Xu, X. Wang, S. H. Wang, C. F. Pan, C. J. Lin and Z. L. Wang, *J. Am. Chem. Soc.*, 2012, **134**, 4437–4441.
15 T.-S. Kang, A. P. Smith, B. E. Taylor and M. F. Durstock, *Nano Lett.*, 2009, **9**, 601–606.
16 D. Kuang, J. Brillet, P. Chen, M. Takata, S. Uchida, H. Miura, K. Sumioka, S. M. Zakeeruddin and M. Graetzel, *ACS Nano*, 2008, **2**, 1113–1116.
17 L. Chen, W. Tan, J. Zhang, X. Zhou, X. Zhang and Y. Lin, *Electrochim. Acta*, 2010, **55**, 3721–3726.
18 X. M. Fang, T. L. Ma, M. Akiyama, G. Q. Guan, S. Tsunematsu and E. Abe, *Thin Solid Films*, 2005, **472**, 242–245.
19 S. Ito, N.-L. C. Ha, G. Rothenberger, P. Liska, P. Comte, S. M. Zakeeruddin, P. Pechy, M. K. Nazeeruddin and M. Graetzel, *Chem. Commun.*, 2006, 4004–4006, DOI: 10.1039/b608279c.
20 H. Sun, Y. Luo, Y. Zhang, D. Li, Z. Yu, K. Li and Q. Meng, *J. Phys. Chem. C*, 2010, **114**, 11673–11679.
21 A. Kumar and C. W. Zhou, *ACS Nano*, 2010, **4**, 11–14.
22 D. Pugliese, A. Lamberti, F. Bella, A. Sacco, S. Bianco and E. Tresso, *Org. Electron.*, 2014, **15**, 3715–3722.
23 N. O. Weiss, H. L. Zhou, L. Liao, Y. Liu, S. Jiang, Y. Huang and X. F. Duan, *Adv. Mater.*, 2012, **24**, 5782–5825.
24 S. R. Ye, A. R. Rathmell, Z. F. Chen, I. E. Stewart and B. J. Wiley, *Adv. Mater.*, 2014, **26**, 6670–6687.
25 M. Zhang, S. L. Fang, A. A. Zakhidov, S. B. Lee, A. E. Aliev, C. D. Williams, K. R. Atkinson and R. H. Baughman, *Science*, 2005, **309**, 1215–1219.
26 D. S. Hecht, L. B. Hu and G. Irvin, *Adv. Mater.*, 2011, **23**, 1482–1513.
27 K. S. Kim, Y. Zhao, H. Jang, S. Y. Lee, J. M. Kim, K. S. Kim, J. H. Ahn, P. Kim, J. Y. Choi and B. H. Hong, *Nature*, 2009, **457**, 706–710.
28 B. J. Lee and G. H. Jeong, *Appl. Phys. A: Mater. Sci. Process.*, 2013, **110**, 29–34.
29 G. Veerappan, K. Bojan and S. W. Rhee, *ACS Appl. Mater. Interfaces*, 2011, **3**, 857–862.
30 J. G. Nam, Y. J. Park, B. S. Kim and J. S. Lee, *Scr. Mater.*, 2010, **62**, 148–150.
31 T. N. Murakami, S. Ito, Q. Wang, M. K. Nazeeruddin, T. Bessho, I. Cesar, P. Liska, R. Humphry-Baker, P. Comte, P. Pechy and M. Gratzel, *J. Electrochem. Soc.*, 2006, **153**, A2255–A2261.
32 J. D. Roy-Mayhew, D. J. Bozym, C. Punckt and I. A. Aksay, *ACS Nano*, 2010, **4**, 6203–6211.
33 J. M. Kroon, N. J. Bakker, H. J. P. Smit, P. Liska, K. R. Thampi, P. Wang, S. M. Zakeeruddin, M. Gratzel, A. Hinsch, S. Hore, U. Wurfel, R. Sastrawan, J. R. Durrant, E. Palomares, H. Pettersson, T. Gruszecki, J. Walter, K. Skupien and G. E. Tulloch, *Prog. Photovoltaics*, 2007, **15**, 1–18.
34 M. Gerosa, A. Sacco, A. Scalia, F. Bella, A. Chiodoni, M. Quaglio, E. Tresso and S. Bianco, *EPJ Photovoltaics*, 2016, **6**, 498–505.
35 B. Anothumakkool, I. Agrawal, S. N. Bhange, R. Soni, O. Game, S. B. Ogale and S. Kurungot, *ACS Appl. Mater. Interfaces*, 2016, **8**, 553–562.
36 K. S. Lee, H. K. Lee, D. H. Wang, N. G. Park, J. Y. Lee, O. O. Park and J. H. Park, *Chem. Commun.*, 2010, **46**, 4505–4507.
37 W. Ke, G. Fang, H. Tao, P. Qin, J. Wang, H. Lei, Q. Liu and X. Zhao, *ACS Appl. Mater. Interfaces*, 2014, **6**, 5525–5530.
38 S. Nagarajan, P. Sudhagar, V. Raman, W. Cho, K. S. Dhathathreyan and Y. S. Kang, *J. Mater. Chem. A*, 2013, **1**, 1048–1054.
39 S. Yun, A. Hagfeldt and T. Ma, *Adv. Mater.*, 2014, **26**, 6210–6237.
40 T.-L. Zhang, H.-Y. Chen, C.-Y. Su and D.-B. Kuang, *J. Mater. Chem. A*, 2013, **1**, 1724–1730.
41 M. Al-Mamun, J.-Y. Kim, Y.-E. Sung, J.-J. Lee and S.-R. Kim, *Chem. Phys. Lett.*, 2013, **561–562**, 115–119.
42 D. Angmo and F. C. Krebs, *J. Appl. Polym. Sci.*, 2013, **129**, 1–14.
43 H. Wu, D. S. Kong, Z. C. Ruan, P. C. Hsu, S. Wang, Z. F. Yu, T. J. Carney, L. B. Hu, S. H. Fan and Y. Cui, *Nat. Nanotechnol.*, 2013, **8**, 421–425.
44 K. D. Yuan, J. J. Wu, M. L. Liu, L. L. Zhang, F. F. Xu, L. D. Chen and F. Q. Huang, *Appl. Phys. Lett.*, 2008, 93.
45 P. Parreira, G. Lavareda, J. Valente, F. T. Nunes, A. Amaral and C. N. de Carvalho, *Phys. Status Solidi A*, 2010, **207**, 1652–1654.

46 P. Parreira, G. Lavareda, A. Amaral, A. M. B. do Rego, O. Conde, J. Valente, F. Nunes and C. N. de Carvalho, *J. Alloys Compd.*, 2011, **509**, 5099–5104.
47 J. Y. Lin, W. Y. Wang, Y. T. Lin and S. W. Chou, *ACS Appl. Mater. Interfaces*, 2014, **6**, 3357–3364.
48 C. Q. Ye, R. G. Hu, S. G. Dong, X. J. Zhang, R. Q. Hou, R. G. Du, C. J. Lin and J. S. Pan, *J. Electroanal. Chem.*, 2013, **688**, 275–281.
49 W. X. Guo, X. J. Zhang, R. M. Yu, M. L. Que, Z. M. Zhang, Z. W. Wang, Q. L. Hua, C. F. Wang, Z. L. Wang and C. F. Pan, *Adv. Energy Mater.*, 2015, 5.